PROPELLER-EPI With Parallel Imaging Using a Circularly Symmetric Phased-Array RF Coil at 3.0 T: Application to High-Resolution Diffusion Tensor Imaging

Tzu-Chao Chuang,[1] Teng-Yi Huang,[2] Fa-Hsuan Lin,[3] Fu-Nien Wang,[1] Chun-Jung Juan,[1,4] Hsiao-Wen Chung,[1*] Cheng-Yu Chen,[4] and Kenneth K. Kwong[3]

A technique integrating multishot periodically rotated overlapping parallel lines with enhanced reconstruction (PROPELLER) and parallel imaging is presented for diffusion echo-planar imaging (EPI) at high spatial resolution. The method combines the advantages of parallel imaging to achieve accelerated sampling along the phase-encoding direction, and PROPELLER acquisition to further decrease the echo train length (ETL) in EPI. With an eight-element circularly symmetric RF coil, a parallel acceleration factor of 4 was applied such that, when combined with PROPELLER acquisition, a reduction of geometric distortions by a factor substantially greater than 4 was achieved. The resulting phantom and human brain images acquired with a 256 × 256 matrix and an ETL of only 16 were visually identical in shape to those acquired using the fast spin-echo (FSE) technique, even without field-map corrections. It is concluded that parallel PROPELLER-EPI is an effective technique that can substantially reduce susceptibility-induced geometric distortions at high field strength. Magn Reson Med 56:1352–1358, 2006.

Key words: PROPELLER imaging; parallel imaging; high-resolution diffusion image; PROPELLER-EPI; geometric distortions

Because it offers rapid data acquisition and requires only a few RF pulses, single-shot echo-planar imaging (EPI) is generally used as the signal readout for diffusion-weighted MRI (DWI). However, owing to EPI's relatively slow sampling rate along the phase-encoding direction, diffusion images generally exhibit substantial susceptibility-related geometric distortions along the phase-encoding direction, especially around regions that show inhomogeneous magnetic field distributions (1). These distortions can strongly degrade the quality of neurological investigations near the skull base, and may result in a misleading clinical diagnosis (2).

[1]Department of Electrical Engineering, National Taiwan University, Taipei, Taiwan, R.O.C.

[2]Department of Electrical Engineering, National Taiwan University of Science and Technology, Taipei, Taiwan, R.O.C.

[3]Massachusetts General Hospital, MGH/MIT/HMS Athinoula A. Martinos Center for Biomedical Imaging, Charlestown, Massachusetts, USA.

[4]Department of Radiology, Tri-Service General Hospital and National Defense Medical Center, Taipei, Taiwan, R.O.C.

Grant sponsor: National Science Council; Grant numbers: NSC-94-2314-B-002-027; NSC-94-2213-E-011-067

Presented in part at the 12th Annual Meeting of ISMRM, Kyoto, Japan, 2004, and the 13th Annual Meeting of ISMRM, Miami Beach, FL, USA, 2005.

*Correspondence to: Hsiao-Wen Chung, Ph.D., Professor, Department of Electrical Engineering, National Taiwan University, Taipei, Taiwan, R.O.C. E-mail: chung@cc.ee.ntu.edu.tw

Received 15 December 2005; revised 13 June 2006; accepted 23 July 2006.
DOI 10.1002/mrm.21064
Published online 18 October 2006 in Wiley InterScience (www.interscience.wiley.com).

Methods to reduce geometric distortion can be divided into at least two different categories. The single-shot approach involves an increase in the bandwidth along the phase-encoding direction (BW_{PE}) by acquiring sufficient data for image reconstruction with a reduced echo train length (ETL) within one shot. A typical example is parallel imaging employing the use of phased-array RF coils (3,4). In contrast to the single-shot approach, methods in the second category reduce the ETL by splitting the entire data acquisition into multiple shots. In multishot diffusion imaging, the phase difference induced by physiological motion in each shot can lead to severe ghosting artifacts (5), since any motion is transformed into a phase change of the spin isochromats after DW magnetization preparation. Therefore, in multishot DWI, robust correction techniques must accompany the acquisition. One technique that could achieve this aim via inherent navigator correction is the multishot periodically rotated overlapping parallel lines with enhanced reconstruction (PROPELLER) method (6,7).

In the present study we integrated the two aforementioned approaches (parallel imaging and PROPELLER acquisition) to obtain multishot high-resolution diffusion images with substantially reduced geometric distortions. We were particularly interested in the PROPELLER imaging method because, as will be shown in a later section, it fills the *k*-space by using several acquisitions of parallel lines around the center *k*-space with rotated phase-encoding directions (7). The rotational symmetry of *k*-space trajectory is especially suitable for parallel imaging acceleration when a circularly symmetric phase array coil is used for signal receiving. In other words, not is only the BW_{PE} increased, the ETL can also be reduced. Although fast spin-echo (FSE), gradient-echo (GRE), or SE techniques have been used as the signal readout module in different versions of PROPELLER imaging (7,8), we chose to use PROPELLER-EPI (9) in our studies on a 3.0 Tesla system to further reduce the RF specific absorption rate (SAR). The results from both phantom and human studies are presented here.

MATERIALS AND METHODS

Pulse Sequence Development

The PROPELLER-EPI method (9) collects data in a series of rotating "blades" to fill the entire *k*-space (Fig. 1). Each blade in *k*-space consists of several parallel lines acquired by the single-shot EPI technique. Figure 1 shows a blade containing a group of *W* lines with *L* sample points in each line and a rotation angle of θ. This means that an image

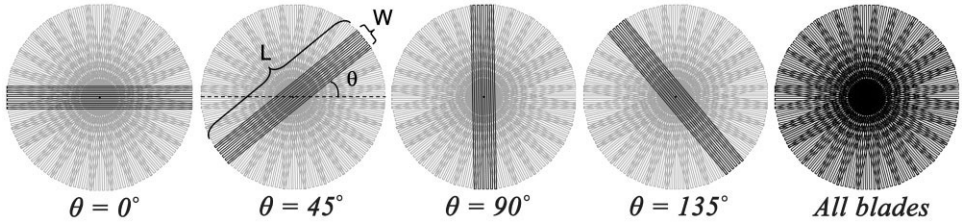

FIG. 1. Schematic drawing of the *k*-space trajectory for PROPELLER-EPI. The data were collected using a series of rotating blades, each containing *W* phase-encoding lines and *L* frequency-encoding sample points acquired using single-shot EPI. Filling of the *k*-space in PROPELLER imaging was accomplished by combining different blades of data at different rotation angles.

with a matrix size of $L \times W$ can be transformed from one blade of the *k*-space data. In its simplest implementation, the *k*-space can be completely filled by combining blades of identical size but at different rotation angles. As a result, the coverage of data in the *k*-space and the FOV of a PROPELLER image are both circular. To fill out the entire *k*-space without causing artifacts from data omission (10), the maximum rotation angle increment ($\Delta\theta$ between two adjacent blades) is $2 \cdot \tan^{-1}(W/L)$, with the minimum number of blades being $\pi/\Delta\theta$.

The incorporation of parallel imaging acceleration into the PROPELLER-EPI method is somewhat different from other acquisition techniques. Specifically, parallel imaging has to be carried out within each blade because the phase-encoding direction varies with the rotating blade, which should be individually reconstructed to full FOV before other processing steps are applied (11). In other words, each blade of *k*-space data is acquired using single-shot EPI at a higher BW_{PE} by skipping certain phase-encoding lines in the EPI trajectory (12,13). The undersampled *k*-space is then unfolded using parallel imaging reconstruction algorithms (12–14), after which the PROPELLER *k*-space data combination is accomplished (Fig. 2). Several properties of the proposed technique should be noted. First, parallel imaging does not really reduce the total scan time, since the acquisition is multishot in nature. Instead, scan time reduction is achieved only within the individual blades. Second, by reducing scan time for all of the single-shot EPI blades, one can reduce geometric distortions by a factor of the parallel acceleration factor. Third, since the phase-encoding directions in PROPELLER spread over the entire circular *k*-space, the best arrangement of the RF phased-array coil elements for a transaxial brain scan is circularly symmetric.

In addition to the signal readout module using parallel PROPELLER-EPI, we employed diffusion weighting using SE-EPI with twice-refocused preparation to minimize eddy-current effects (15).

Image Reconstruction

Reconstruction of the images consisted of two parts: parallel imaging and PROPELLER-EPI reconstructions. In this study the parallel imaging unfolding procedure preceded the PROPELLER data combination (Fig. 2). The image domain algorithm sensitivity encoding (SENSE) (12) and the *k*-space domain algorithm generalized autocalibrating partially parallel acquisitions (GRAPPA) (14) were both applied for parallel imaging unfolding using vendor-equipped software. To demonstrate the advantage of PROPELLER reconstruction in the presence of parallel imaging unfolding artifacts, one set of phantom data were intentionally reconstructed using less-dedicated SENSE software developed in-house. The sensitivity profiles of individual coil elements were merely estimated by applying a low-pass filter on a preacquired full-FOV reference EPI image without registering to the imaged object or using regularization (16). After SENSE or GRAPPA processing,

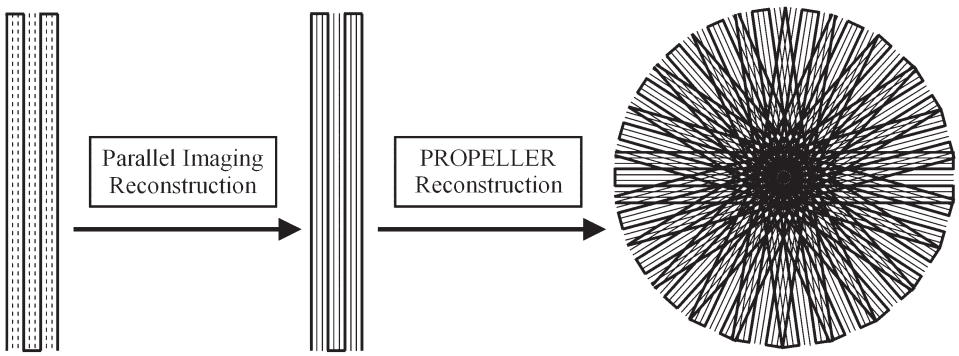

FIG. 2. The drawing shows the reconstruction procedure for parallel PROPELLER-EPI, in which PROPELLER reconstruction was applied following parallel reconstruction. On the left, one blade of data was acquired by single-shot EPI (thick solid lines) with phase-encoding skipped (dashed lines, threefold acceleration in this example). After parallel imaging unfolding was performed, the missing data were filled (middle, thin solid lines). Subsequently, all of the blades were combined to fill the entire circular *k*-space using the PROPELLER reconstruction procedure (right).

the unaliased *k*-space data of all of the blades underwent PROPELLER reconstruction procedures following the steps described in Ref. 9. This process consisted of spatial registration of low-resolution blade images, phase correction to avoid destructive interference during data combination, triangular windowing to reduce off-resonance effects, and density compensation to achieve uniform weighting of the *k*-space data. Note that since both parallel imaging and PROPELLER help to reduce geometric distortions, we did not use further off-resonance corrections with field maps (1,9) in this study.

Imaging Experiments

Imaging experiments were performed at 3.0 Tesla on two whole-body MR scanners (Magnetom Trio, Siemens, Erlangen, Germany, maximum gradient strength = 40 mT/m, maximum gradient slew rate = 200 mT/m/ms; and Achieva, Philips, Best, The Netherlands, maximum gradient strength = 80 mT/m, maximum gradient slew rate = 100 mT/m/ms). For all experiments, the receiver head coil was a circularly symmetric phased array, with similar spatial arrangements of the eight coil elements. A resolution phantom was scanned to demonstrate the image quality of the combination of parallel imaging with PROPELLER-EPI. For this purpose, seven PROPELLER blades of *k*-space data were acquired. A single-shot SE-EPI scan (FOV = 220 mm, TR/TE = 1000/50 ms) with 256 frequency-encoding samples, and spaced at 26° from adjacent blades to cover a circular *k*-space, was used for each blade. Four different SENSE acceleration factors (R = 1, 2, 2.6, and 4) were used to acquire the signals to reconstruct 64 lines in *k*-space for each blade. The corresponding ETLs were thus 64, 32, 24, and 16, respectively. No diffusion gradient was applied in the phantom study.

In addition to the phantom study, experiments on human brains in vivo were also performed. Fourteen healthy adults (12 males and two females, 20–29 years old) with no history of brain disease volunteered for this study. The in vivo study was approved by the internal review board of our hospital, and written informed consent was obtained from all subjects before the experiments. For each volunteer, a clinical turbo SE (TSE) sequence (TR/TE = 3440/102 ms, ETL = 9, NEX = 1, matrix size = 384 × 384, FOV = 220 × 220 mm^2, thickness = 5 mm) was first applied to obtain 10 slices of T2-weighted images as the reference standard with no geometric distortions. Second, PROPELLER spin-echo EPI with GRAPPA was performed to acquire anatomical images. The imaging parameters included TR = 2 s, 14 blades spaced at 13° from adjacent blades, four averages, blade size = 64 × 256, FOV = 220 mm, and slice thickness = 5 mm. The ETL of each PROPELLER blade was further reduced using the GRAPPA technique, with reduction factors of 1, 2, and 4. Due to ETL reduction, the minimum achievable TE of each blade was reduced accordingly. Consequently, TEs of 135 ms, 89 ms, and 71 ms were used for GRAPPA reduction factors R of 1, 2, and 4 (corresponding to ETLs of 64, 32, and 16), respectively. After all of the blades were combined by the PROPELLER reconstruction method, the final images had a nominal in-plane resolution of 0.86 × 0.86 mm^2.

Following anatomical imaging with GRAPPA PROPELLER-EPI, diffusion magnetization-prepared PROPELLER-EPI was applied at the identical slice location as in the previous scan to obtain DW images in six different diffusion directions ((x, y, z) = (1,1,0), (1,–1,0), (1,0,1), (1,0,–1), (0,1,1), (0,1,–1), with a b-value of 700 s/mm^2), plus one image set with the diffusion gradient switched off to obtain a b = 0 reference. The diffusion data were acquired only with three- to fourfold acceleration, four to six averages, and TE = 85 ms. All of the other parameters were kept the same as for the anatomical scan.

RESULTS

Phantom Trial

Figure 3 shows images acquired from the resolution phantom using PROPELLER-EPI with in-house SENSE reconstruction at different acceleration factors (R = 1, 2, 2.6, and 4, from left to right). For comparison purposes, two out of seven low-resolution images reconstructed from single-blade data are presented in the upper and middle rows, respectively. It can be seen that the EPI-related geometric distortions differ in orientation. The upper images appear to be elongated along the vertical direction, whereas images in the middle row show compression along an oblique-vertical direction. The difference was especially prominent when SENSE acceleration was not used (i.e., R = 1), and became less noticeable as R increased. These differently oriented geometric distortions led to blurring effects in the final PROPELLER images reconstructed from all seven blades of data, as shown in the bottom row of Fig. 3. At high reduction factors, blurring was substantially reduced due to decreased distortions in the low-resolution blade images, while the signal-to-noise ratio (SNR) decreased because of a reduction in the acquisition matrix size. Nevertheless, the sacrifice in SNR was compensated for by the visual absence of blurring effects at R = 4, which improved the overall image quality. In addition, the unfolding ghosts that are commonly seen in imperfectly SENSE-reconstructed images became distributed in all directions, with prominently reduced amplitude in the PROPELLER-EPI images, which led to improved signal uniformity within the phantom compared to the single-blade images.

Volunteer Experiments

Figure 4 shows one image slice obtained from a 24-year-old subject. Images in the upper row were single-blade EPI scans with the GRAPPA parallel imaging technique at acceleration factors R = 1 (Fig. 4a), 2 (Fig. 4b), and 4 (Fig. 4c), respectively. The phase-encoding direction was anterior–posterior. The distortions particularly prominent in the frontal lobe are shown to reduce as the acceleration factor increases. The PROPELLER-EPI images at corresponding acceleration factors are shown in Fig. 4d–f, with Fig. 4g showing the TSE image for comparison. Note that the PROPELLER-EPI images demonstrate improved preservation of geometric shape compared to their single-blade counterparts, as evidenced by a comparison with the TSE image in Fig. 4g. In addition, in the presence of severe field heterogeneity, which hampered PROPELLER reconstruction and yielded the artifacts shown in Fig. 4d, parallel imaging further reduced the artifacts. At R = 4, the PRO-

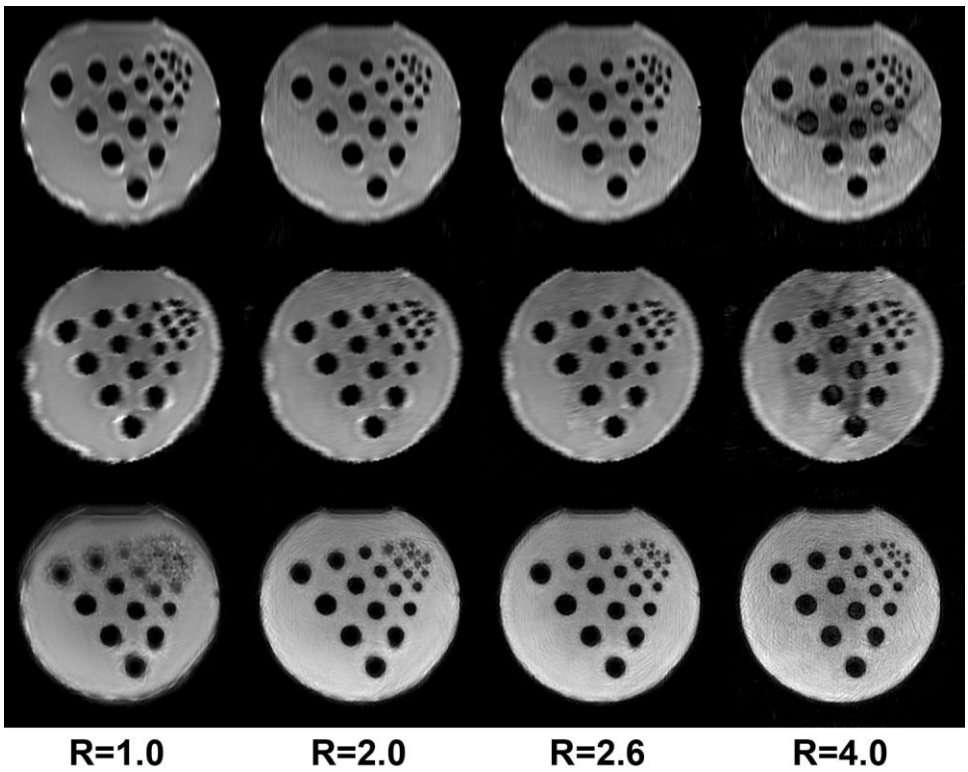

FIG. 3. Phantom images acquired with PROPELLER-EPI with SENSE acceleration by factors of $R = 1$ (i.e., no SENSE acceleration), 2, 2.6, and 4 (from left to right, respectively). In each column the upper and middle images show two low-resolution images reconstructed from single blades, with phase-encoding directions differing by 78°. The lower images are the corresponding PROPELLER images reconstructed from all seven blades. Note the improved morphology as R increases, and the improved signal uniformity through PROPELLER reconstruction as compared to the single-blade images even in the presence of SENSE unfolding ghosts at $R = 4$ (right column). In addition, as R increases, the SNR decreases. However, this is compensated for by the absence of blurring effects, as evidenced by the clarity of small dots at high acceleration factors.

PELLER-EPI image in Fig. 4f exhibits little visual difference from the TSE image (Fig. 4g) in terms of geometry. At the skull-base region, where the susceptibility effects are relatively stronger, the technique still gave a satisfactory performance even without any field-map corrections. This is illustrated in Fig. 5 which shows the high-resolution DW images of a 23-year-old female subject for six consecutive slices near the skull base, acquired using PROPEL-

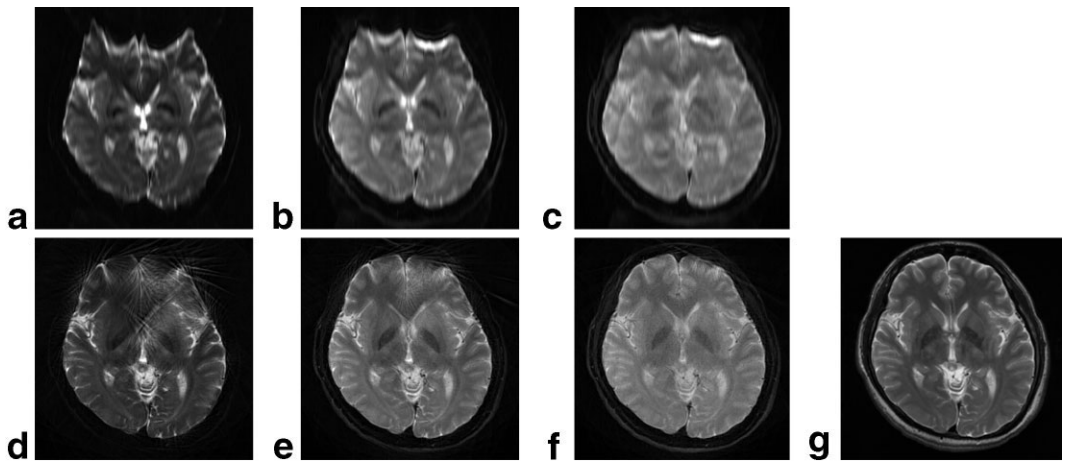

FIG. 4. Comparison of the effects of PROPELLER reconstruction and GRAPPA parallel imaging on one image obtained from a 24-year-old male subject. Upper row: Low-resolution images from single-blade data. Bottom row (except for **g**): PROPELLER images reconstructed from 14 blades of data. Left to right: Images in columns **a** and **d**, **b** and **e**, and **c** and **f** were acquired with GRAPPA acceleration with reduction factors of $R = 1$, 2, and 4, respectively. The image in g is the FSE image at the identical slice selection. Both PROPELLER imaging and parallel acceleration substantially reduced geometric distortions near the frontal lobe. The difference in contrast was due to the difference in TEs.

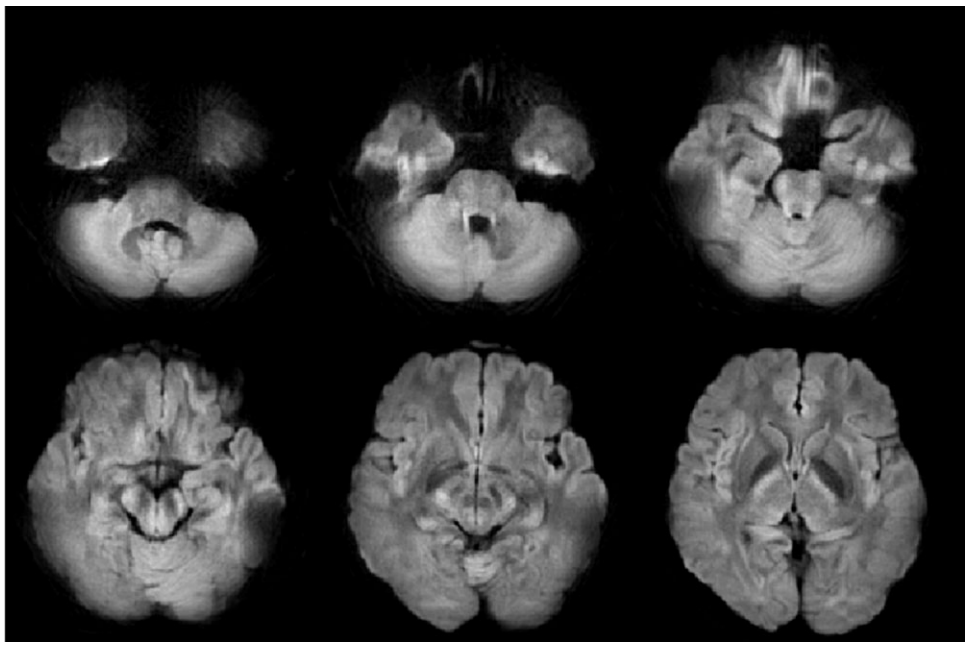

FIG. 5. Six DWI slices from a 23-year-old female subject, which were acquired using PROPELLER-EPI with GRAPPA parallel imaging at an acceleration factor of 3. The diffusion gradient was along the direction of (x, y, z) = (0, 1, 1) at a b-value of 700 s/mm^2.

LER-EPI with GRAPPA at $R = 3$ and NEX = 6. The diffusion gradient was along the direction of (0,1,1) at a b-value of 700 s/mm^2.

Figure 6 shows the color-encoded fractional anisotropy (FA) maps of a 21-year-old subject, which were acquired with threefold GRAPPA acceleration and six averages. Not only are the orientations of the major eigenvectors clearly visualized from the high-resolution color mapping (red: left–right, green: anterior–posterior, blue: cranial–caudal), but many of the anatomic structures of white matter can also be identified from the color-encoded FA maps alone. The identifiable anatomy includes the superior and inferior longitudinal fasciculus (SLF and ILF), arcuate fasciculus (AF), genu and splenium of corpus callosum (CC), anterior and posterior limbs of the internal capsules (ALIC and PLIC), external capsules (EC), corticospinal tracts (CST), corona radiate (CR), tapetum (TP), cigulum (CG), optic tracts (OT), and optic radiation (OR) (Fig. 6).

DISCUSSION

In this study we have presented a technique that is suitable for high-resolution DWI. PROPELLER acquisition and par-

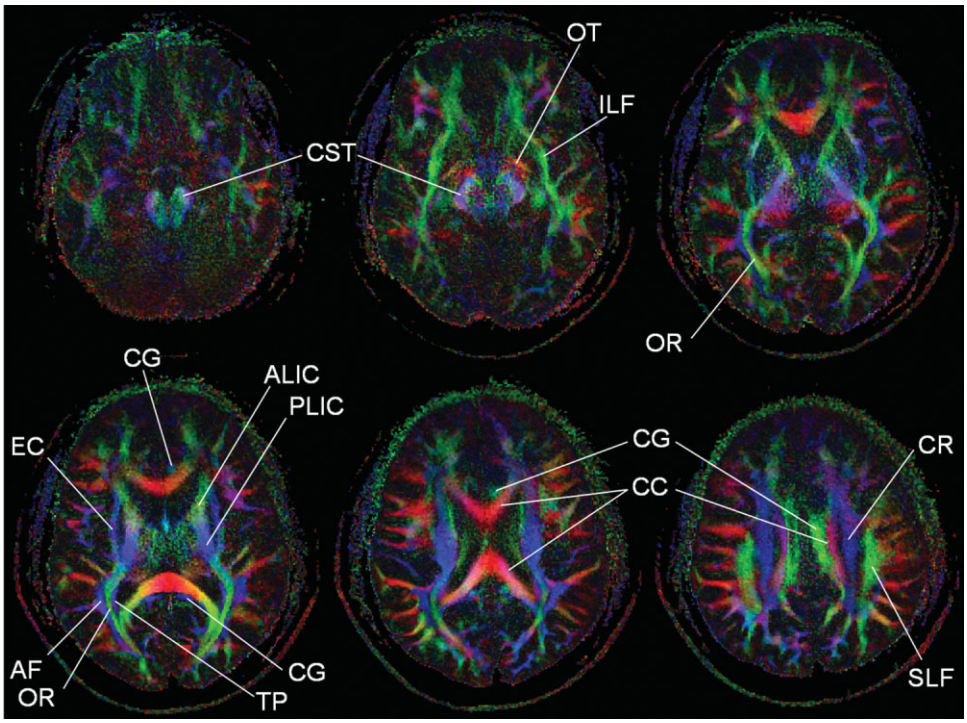

FIG. 6. Color-encoded FA maps for a 21-year-old subject (red: left–right, green: anterior–posterior, blue: cranial–caudal). The white-matter anatomical structures that are identifiable from these maps alone are indicated by white solid lines and corresponding text.

alleling imaging methods were simultaneously employed to reduce the distortions and artifacts that would be seen on conventional DW single-shot EPI images. Using a circularly symmetric eight-channel head coil, we demonstrated that a parallel acceleration factor of up to 4 can be achieved for all individual rotating blades in PROPELLER-EPI, thus giving an ETL of only 16 during single-blade acquisitions to yield a 256 × 256 image. As a consequence, susceptibility-induced geometric distortions due to a slow sampling rate along the phase-encoding direction were substantially reduced. Both phantom and in vivo experiments demonstrated that the parallel PROPELLER-EPI images showed similar quality in most of the brain region when compared with the distortion-free FSE images as references.

Diffusion imaging and parallel techniques have been combined in many previous applications (3,4). However, one should note that the maximum acceleration factor is restricted to the number of RF coil elements that exhibit independent sensitivity profiles along the phase-encoding direction (13). To the best of our knowledge, an acceleration factor of <4 is generally used for a circularly symmetric coil containing eight elements arranged in a similar manner to that used in our study. In other words, the ETL in parallel EPI cannot be unlimitedly reduced. A fourfold acceleration would still necessitate the acquisition of 64 echoes to obtain an image with a 256 × 256 matrix. On the other hand, the incorporation of the PROPELLER acquisition technique with parallel EPI further reduced the ETL. At least in this study, a reduction of the ETL by another factor of 4 was demonstrated successfully in both phantom and in vivo brain images. The resulting factor-of-16 difference in ETL shows that the combined parallel PROPELLER-EPI method provides significant benefits, as evidenced by the experimental results in which geometric distortions were found to be reduced by a factor substantially greater than 4. Similar advantages from parallel imaging should also be obtainable for the recently reported variation of PROPELLER-EPI using a short-axis readout (17).

It is noted that image warping arising from eddy currents in the presence of strong diffusion gradients behaves in a different manner compared to susceptibility-induced geometric distortions. While the use of parallel imaging could reduce eddy-current warping (4), the registration procedure used in the PROPELLER-EPI method can only eliminate the shifting displacements from residual gradients along the slice direction. Scaling and shearing from residual gradients along the phase and frequency directions (18), on the other hand, would transform into blurring in the final PROPELLER-reconstructed images if retrospective non-rigid corrections were not performed (19). This is different from susceptibility distortions, for which PROPELLER reconstruction and parallel imaging both help to reduce the off-resonance effects. It is therefore beneficial to minimize eddy-current effects by means of an optimized pulse sequence design, such as the twice-refocused scheme used in this study (15).

Reducing the ETL in an EPI acquisition can also lead to improvements in the SNR and reduce blurring effects. In the DWI experiments we were able to shorten the TE from 135 ms to 71 ms as the parallel acceleration factor increased from 1 to 4. Given that white matter has a T_2 of approximately 70 ms at 3.0 Tesla (20), the signal intensity gain from the TE shortening is approximately 2.5-fold. Furthermore, a short ETL at constant echo spacing reduced point-spread function (PSF) blurring, which can arise from T_2* decay throughout the entire signal readout period.

Compared to segmented EPI techniques, it is more beneficial to use PROPELLER-EPI as the signal readout module because in addition to the suitability of parallel imaging acceleration with a circularly symmetric array coil, any unfolding artifacts that might arise from an imperfect parallel imaging reconstruction became relatively invisible (cf., Fig. 3). In fact, the unfolding artifacts in parallel imaging manifest themselves as ghosts along the phase-encoding direction. Because the PROPELLER *k*-space trajectory exhibits different phase-encoding directions in all blades, unfolding ghosts become smeared circularly in the image, with each individual ghost reduced in amplitude by a factor equal to the number of blades. This inherently suppresses the unfolding ghosts, in agreement with a previous study in which EPI Nyquist ghosts were shown to be much less prominent in PROPELLER-EPI than in single-shot EPI (9). This issue is illustrated in Fig. 3, where the unfolding artifacts were intentionally magnified using less dedicated SENSE reconstruction software. Note that although the PROPELLER phantom image at $R = 4$ exhibited signal drops at the center due to the presence of unfolding artifacts, the signal uniformity is still better than that obtained with its single-blade counterparts. For SENSE reconstruction using vendor-equipped software, even better signal uniformity, comparable to the level of TSE imaging, is easily obtainable due to further reduction of the unfolding ghosts. In contrast, segmented EPI would be unable to provide reduction of unfolding ghosts because of the lack of a circular *k*-space trajectory.

Peripheral nerve stimulation (PNS) in PROPELLER-EPI is a potential issue that should receive some attention. There is increasing evidence that PNS depends on the gradient direction in addition to the magnitude and duration of dB/dt (21), with a higher occurrence rate along the anterior–posterior direction (22,23). Minimization of PNS in single-shot EPI could thus be achieved by setting the readout direction to left–right. In comparison, however, it is difficult to perform a similar action in PROPELLER-EPI because the frequency-encoding directions vary in every blade and thus include all possible orientations on the transverse plane. In our implementation on two different MR systems, we were able to almost completely avoid PNS on one scanner by regulating the maximum dB/dt before data acquisition, but the presence of PNS was highly reproducible on the other scanner, where our access to the control of dB/dt was relatively restricted. Therefore, a reduction of PNS via careful adjustment of the maximum dB/dt should at least be practiced before the method is used for clinical applications. As a final note, the PNS reported in this article is strictly PROPELLER-EPI-specific and unrelated to the use of parallel imaging.

One limitation of our proposed technique is the lack of flexibility in selecting slice orientations. Although many of the images shown in this study were oblique, they were largely axial. As the slice orientation becomes close to coronal or sagittal, parallel imaging acceleration would

become inappropriate for certain blades in PROPELLER imaging. Possible remedies include newly implemented phased-array coils with elements covering all three acceleration directions (24). However, that would necessitate a modification of the receiver channels and hence is beyond the scope of this study.

CONCLUSIONS

We conclude that the combination of PROPELLER-EPI acquisition and parallel imaging acceleration is an effective technique that provides substantial reductions in susceptibility-induced geometric distortions, even at high field strength. The technique proposed in this work is suitable for diffusion imaging with high spatial resolution.

REFERENCES

1. Chen NK, Wyrwicz AM. Optimized distortion correction technique for echo planar imaging. Magn Reson Med 2001;45:525–528.
2. Forbes KP, Pipe JG, Karis JP, Heiserman JE. Improved image quality and detection of acute cerebral infarction with PROPELLER diffusion-weighted MR imaging. Radiology 2002;225:551–555.
3. Jaermann T, Crelier G, Pruessmann KP, Golay X, Netsch T, van Muiswinkel AM, Mori S, van Zijl PC, Valavanis A, Kollias S, Boesiger P. SENSE-DTI at 3 T. Magn Reson Med 2004;51:230–236.
4. Bammer R, Auer M, Keeling SL, Augustin M, Stables LA, Prokesch RW, Stollberger R, Moseley ME, Fazekas F. Diffusion tensor imaging using single-shot SENSE-EPI. Magn Reson Med 2002;48:128–136.
5. Golay X, Jiang H, van Zijl PC, Mori S. High-resolution isotropic 3D diffusion tensor imaging of the human brain. Magn Reson Med 2002; 47:837–843.
6. Pipe JG. Motion correction with PROPELLER MRI: application to head motion and free-breathing cardiac imaging. Magn Reson Med 1999;42: 963–969.
7. Pipe JG, Farthing VG, Forbes KP. Multishot diffusion-weighted FSE using PROPELLER MRI. Magn Reson Med 2002;47:42–52.
8. Pipe JG, Zwart N. Turboprop: improved PROPELLER imaging. Magn Reson Med 2006;55:380–385.
9. Wang FN, Huang TY, Lin FH, Chuang TC, Chen NK, Chung HW, Chen CY, Kwong KK. PROPELLER EPI: an MRI technique suitable for diffusion tensor imaging at high field strength with reduced geometric distortions. Magn Reson Med 2005;54:1232–1240.
10. Arfanakis K, Tamhane AA, Pipe JG, Anastasio MA. k-Space undersampling in PROPELLER imaging. Magn Reson Med 2005;53:675–683.
11. Pipe JG. The use of parallel imaging with PROPELLER DWI. In: Proceedings of the 11th Annual Meeting of ISMRM, Toronto, Canada, 2003. p.66.
12. Pruessmann KP, Weiger M, Scheidegger MB, Boesiger P. SENSE: sensitivity encoding for fast MRI. Magn Reson Med 1999;42:952–962.
13. Sodickson DK, Manning WJ. Simultaneous acquisition of spatial harmonics (SMASH): fast imaging with radiofrequency coil arrays. Magn Reson Med 1997;38:591–603.
14. Griswold MA, Jakob PM, Heidemann RM, Nittka M, Jellus V, Wang J, Kiefer B, Haase A. Generalized autocalibrating partially parallel acquisitions (GRAPPA). Magn Reson Med 2002;47:1202–1210.
15. Reese TG, Heid O, Weisskoff RM, Wedeen VJ. Reduction of eddy-current-induced distortion in diffusion MRI using a twice-refocused spin echo. Magn Reson Med 2003;49:177–182.
16. Lin FH, Kwong KK, Belliveau JW, Wald LL. Parallel imaging reconstruction using automatic regularization. Magn Reson Med 2004;51: 559–567.
17. Skare S, Newbould RD, Clayton DB, Bammer R. Propeller EPI in the other direction. Magn Reson Med 2006;55:1298–1307.
18. Jezzard P, Barnett AS, Pierpaoli C. Characterization of and correction for eddy current artifacts in echo planar diffusion imaging. Magn Reson Med 1998;39:801–812.
19. Netsch T, van Muiswinkel A. Quantitative evaluation of image-based distortion correction in diffusion tensor imaging. IEEE Trans Med Imaging 2004;23:789–798.
20. Stanisz GJ, Odrobina EE, Pun J, Escaravage M, Graham SJ, Bronskill MJ, Henkelman RM. T1, T2 relaxation and magnetization transfer in tissue at 3T. Magn Reson Med 2005;54:507–512.
21. Budinger TF, Fischer H, Hentschel D, Reinfelder HE, Schmitt F. Physiological effects of fast oscillating magnetic field gradients. J Comput Assist Tomogr 1991;15:909–914.
22. Zhang B, Yen YF, Chronik BA, McKinnon GC, Schaefer DJ, Rutt BK. Peripheral nerve stimulation properties of head and body gradient coils of various sizes. Magn Reson Med 2003;50:50–58.
23. Bourland JD, Nyenhuis JA, Schaefer DJ. Physiologic effects of intense MR imaging gradient fields. Neuroimaging Clin N Am 1999;9:363–377.
24. Wiggins GC, Potthast A, Triantafyllou C, Lin FH, Benner T, Wiggins CJ, Wald L. A 96-channel MRI system with 23- and 90- channel phase array head coils at 1.5 Tesla. In: Proceedings of the 13th Annual Meeting of ISMRM, Miami Beach, FL, USA, 2005. p 671.